Video reflectometry to specify optical properties of tissue in vivo

Steven Jacques

Steven Jacques, "Video reflectometry to specify optical properties of tissue in vivo," Proc. SPIE 10311, Medical Optical Tomography: Functional Imaging and Monitoring, 103110D (5 August 1993); doi: 10.1117/12.2283758

SPIE.

Event: Medical Optical Tomography: Functional Imaging and Monitoring, 1993, Bellingham, WA, United States

Video Reflectometry to Specify Optical Properties of Tissue *in vivo*.

Steven Jacques 1,2
Achim Gutsche 1,2
Jon Schwartz 1
Lihong Wang 1
Frank Tittel 2

1. Laser Biology Research Laboratory
University of Texas M. D. Anderson Cancer Center
1515 Holcombe Blvd., Houston, Texas 77030

2. Department of Electrical and Computer Engineering,
Rice University, Houston, Texas 77030

INTRODUCTION

The measurement of tissue optical properties is often required for proper design of therapeutic or diagnostic uses of light in medicine. The ability of light to spread into a tissue and the rate of light absorption by the tissue are two related but distinct processes. The two independent optical parameters which affect these processes are absorption and scattering. To understand light propagation, two independent optical measurements must be made. In this paper, we discuss the measurements of total diffuse reflectance and lateral spread of light in response to a point source of irradiance. In this paper, we call this technique "video reflectometry".

The video reflectometry technique is a noncontact measurement. Therefore, it can be used with living tissues with their *in situ* water balance and blood content. The technique includes two measurements: (1) a photodiode measurement of total diffuse reflectance, R_d, and (2) a video camera measurement of the lateral spread of light in the tissue which is expressed as the local diffuse reflectance, R(r). Although it is possible to obtain the value of R_d from the integration of the video R(r) data, the independent photodiode measurement of R_d is more reliable and more easily calibrated. Therefore, we employ the two methods in video reflectometry.

Criteria for successful use of video reflectometry is that the tissue is (1) homogeneous and (2) semi-infinite in thickness. Often both these conditions are met. Depending on the wavelength, light may penetrate only 0.1-10 mm into a tissue. For example, yellow light will not fully penetrate the 2-4-mm-thick dermis and therefore the dermis is optically a semi-infinite tissue at that wavelength.

THEORY

The diffusion of light

The diffusion of light from a point source is described by the fluence rate, ϕ, in cm^{-2}. If the point source delivers 1 W of power, the fluence rate is expressed in W/cm^2.

$$\phi(r) = \frac{1}{4\pi D}\frac{\exp(-r/\delta)}{r} \qquad [1]$$

Medical Optical Tomography: Functional Imaging and Monitoring, edited by Gerhard J. Mueller,
Proc. of SPIE Vol. 10311 (Vol. IS11), 103110D · © (1993) 2017 SPIE
CCC code: 0277-786X/17/$18 · doi: 10.1117/12.2283758

where **r** is the distance from the point source in a homogenous medium which can be expressed in either Cartesian coordinates or, for this paper, in cylindrical coordinates:

$$\mathbf{r} = \sqrt{x^2 + y^2 + z^2} = \sqrt{r^2 + z^2} \quad [2]$$

where r and z are the radial and axial positions relative to the source.

The term D is the *optical diffusion length* in cm. The term δ is the *optical penetration depth*, and is the propagation distance in cm which causes 1/e attenuation of the fluence rate of light due to both absorption and scattering. The relationship between D and δ is given:

$$\delta = \sqrt{\frac{D}{\mu_a}} \quad [3]$$

where μ_a is the absorption coefficient in cm^{-1}. The rate of energy deposition is given by the product $\mu_a\phi$. If one integrates the product $\mu_a\phi$ over the entire tissue volume, the total integral equals unity, which satisfies the need for conservation of energy:

$$\int_0^\infty \mu_a \phi(\mathbf{r})\, 4\pi r^2 d\mathbf{r} = 1 \quad [4]$$

Table 1: Summary of definitions

μ_a	cm^{-1}	absorption coefficient
μ_s'	cm^{-1}	reduced scattering coefficient = $\mu_s(1-g)$
μs	cm-1	scattering coefficient
g	---	anisotropy = $<\cos\theta>$
θ	rad	deflection angle of scattering event
D	cm	optical diffusion coefficient
δ	cm	optical penetration depth
$\phi(\mathbf{r})$	cm^{-2}	fluence rate
r	cm	distance from point source
R(r)	cm^{-2}	local diffuse reflectance
r	cm	radial distance from point source
z_o	cm	depth of point source below surface
R_d	---	total diffuse reflectance

Reflectance

Reflectance is the flux of light escaping at a tissue surface. For a moment consider a purely mathematical surface at constant $z = z_o$ within an infinite medium. The outward flux across the surface is equal to minus the diffusion coefficient, D, times the gradient of the flux normal to the surface:

$$\text{outward flux across surface} = -D \frac{\partial \phi(r)}{\partial z} \text{ at surface} \quad [5]$$

Consider two comments on Eq. 5:

(1) Future discussion will be easier if the coordinate system is redefined such that the tissue surface is located at z = 0 and the point source is located at a depth z_o below the surface. In such a coordinate system, the flux across the surface is $+D\partial\phi/\partial z$ rather than $-D\partial\phi/\partial z$.

(2) When discussing reflectance, the tissue is usually a semi-infinite medium, not an infinite medium. There is no backward diffusion into tissue from regions outside the tissue. Therefore, Eq. 1 which describes a single point source within an infinite medium is inappropriate for discussion of a semi-infinite tissue. Farrel et al., 1992.[1] applied the concept of a dipole source consisting of two point sources within an infinite homogeneous tissue; one source is positive and located below the true tissue surface ($z = z_o$) and the other source is negative and located above the true tissue surface (in the region $z < 0$). The positive source pushes light out of the tissue and the negative source pulls light out of the tissue. There is a surface midway between the two point sources where the fluence rate, ϕ, equals zero. Let us call this surface the *zero-value surface*. Because the problem is asymmetrical (tissue on one side of the zero-value surface, no tissue on the other side), the zero-value surface is not located at the true tissue surface but rather is located slightly outside or above the true tissue surface. The reflectance is simply the flux that is driven toward the zero-value surface by the gradient of $\partial\phi/\partial z$ within the tissue, evaluated at the tissue surface:

$$R(r) = +D\frac{\partial\phi(r)}{\partial z}\quad \text{at } z = 0 \qquad [6]$$

The boundary condition at the tissue surface requires that no light diffuses back into the tissue because once light escapes the tissue it is assumed to be lost forever. For the case of a matched boundary condition, the fluence rate at the surface must be related to the outward flux at the surface. Fluence rate indicates the light incident from all directions which crosses an incremental path, dL. In contrast, the outward flux or reflectance indicates the light passing normal to the surface which crosses an incremental path dz per incremental dL. The relation between dL and dz is:

$$dz = \cos\theta\, dL \qquad [7]$$

and when integrated over all the angles of incidence from the hemisphere of diffuse light that strikes the tissue surface from within the tissue, the ratio dL/dz is specified:

$$\frac{dL}{dz} = \frac{\int_0^{\pi/2} 2\pi\sin\theta d\theta}{\int_0^{\pi/2} \cos\theta\, 2\pi\sin\theta d\theta} = \frac{2\pi}{\pi} = 2 \qquad [8]$$

Therefore, there is a factor of 2 when converting from fluence rate to outward flux. The boundary condition can be stated:

$$\phi(r) = 2R(r) = 2D\frac{\partial\phi(r)}{\partial z}\quad \text{at } z = 0 \qquad [9]$$

or

$$\frac{\partial\phi(r)}{\partial z} = \frac{\phi}{2D}$$

If the gradient between the dipole point sources is approximately linear in the region between the zero-value surface and the true tissue surface, then a simple trick is possible. If the zero-value surface is located at z = -2D then the gradient at the true tissue surface will be $\phi(r, z = 0)/2D$. Therefore, by placing the dipole's negative point source at a position $z = -z_o - 4D$, one can establish the proper boundary condition of Eq. 9 at the true tissue surface (see Fig. 1).

For the case of a mismatched boundary condition, the surface presents a mismatch in refractive index, eg., $n_{rel} = n_{tissue}/n_{air} \approx 1.37$, and this mismatched boundary internally reflects about half of the light that reaches the surface. Under such conditions, the boundary condition is given:

$$\phi(r) = 2AD\frac{\partial\phi(r)}{\partial z} \quad \text{at } z = 0 \qquad [10]$$

where

$$A = \frac{1 + r_i}{1 - r_i} \qquad [11]$$

where r_i is the internal reflectance. Groenhuis et al.[2] offer an approximate expression for r_i as a function of n_{rel} based on application of Fresnel reflectance at a mismatched boundary integrated over the hemisphere of diffusely incident light striking the boundary:

$$r_i = 0.668 + 0.0636n + 0.710/n - 1.440/n^2 \qquad [12]$$

Jacques[3] has pointed out that r_i is closely but not accurately described by such a calculation. Photons which obliquely strike the surface are internally reflected but photons which orthogonally the surface escape as observable reflectance, therefore the surface itself alters the radiance near the surface such that the radiance is no longer purely diffuse. Oblique photons tend to concentrate near the surface, which slightly increases r_i. Using Monte Carlo simulations for the case of $n_{rel} = 1.37$ and a plane wave of incident irradiance, Jacques plotted $(\phi(z = 0) - 1)/R_d$ and found that the value of 2A is 7.1 ($r_i = 0.560$) rather than 6.35 ($r_i = 0.521$) as predicted by diffusion theory.

Fig. 1 summarizes the geometry of the dipole model. The positive point source is at $z = z_o$ and the negative point source is at $z = -z_o - 4AD$. Superposition of the point source solution, Eq. 1, applied to these two point sources in an infinite medium will mimic the behavior for a single point source at z_o in a semi-infinite medium.

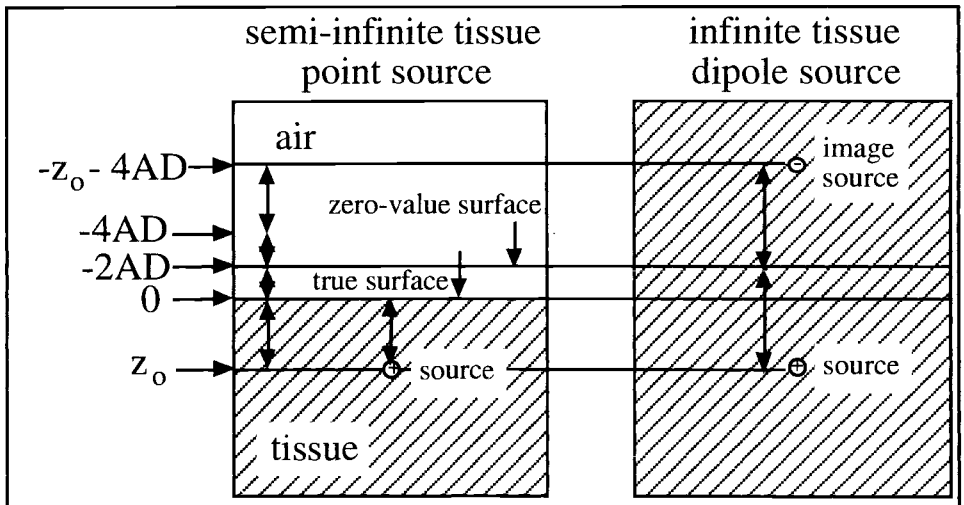

Fig. 1: The dipole model (Farrel et al.[1]) mimics a semi-infinite tissue. A negative image source at position $z = -z_o - 4AD$ establishes a *zero-value surface* at position $z = -2AD$, which asserts the correct boundary condition (Eq. 9) at the *true tissue surface*, $z = 0$. There is an assumption that the gradient of fluence rate for the dipole model is linear in the range $-2AD \le z \le 0$.

R(r), Farrel et al.

The above approach toward reflectance from a semi-infinite medium was proposed by Farrel et al. 1992[1] and the reader is referred to that careful presentation. Their derivation consists of applying Eq. 1 to the two point sources described above and adding the two contributions to yield the solution for $\phi(r, z = 0)$. The first step is to define the **r** of Eq. 1 as $\mathbf{r}_1$ and $\mathbf{r}_2$ for each of the two point sources. Then R(r) equals $D\partial\phi/\partial z$ at $z = 0$, as in Eq. 6, which yields the following expression for the local reflectance, R(r):

$$R(r) = \frac{1}{4\pi}\left[z_o\left(\frac{1}{\delta} + \frac{1}{\mathbf{r}_1}\right)\frac{\exp(-\mathbf{r}_1/\delta)}{\mathbf{r}_1^2} + (z_o + 4AD)\left(\frac{1}{\delta} + \frac{1}{\mathbf{r}_2}\right)\frac{\exp(-\mathbf{r}_2/\delta)}{\mathbf{r}_2^2}\right] \qquad [13]$$

where

$$r_i = 0.668 + 0.0636n + 0.710/n - 1.440/n^2$$

$$A = \frac{1 + r_i}{1 - r_i}$$

$$\mathbf{r}_1 = \sqrt{z_o^2 + r^2}$$

$$\mathbf{r}_2 = \sqrt{(z_o + 4AD)^2 + r^2}$$

The value of D is known from diffusion theory:

$$D = \frac{1}{3(\mu_a + \mu_s')} \quad [14]$$

which specifies the value of δ via Eq. 3:

$$\delta = \sqrt{\frac{D}{\mu_a}} = \frac{1}{\sqrt{3\mu_a(\mu_a + \mu_s')}} \quad [15]$$

In addition, Farrel et al. made a choice for the placement of the point sources by specifying z_o:

$$z_o = \frac{1}{\mu_a + \mu_s'} = 3D \quad [16]$$

This choice for z_o has been shown to be sufficiently deep that the boundary condition does not affect the accuracy of the diffusion theory description of R(r).[4,5] This value for z_o is sometimes called the transport mean free path, or mfp'.

The expression for the total diffuse reflectance is given:

$$R_d = \int_0^\infty R(r)\, 2\pi r dr \quad [17]$$

which by inserting Eq. 13 yields:

$$R_d = \frac{1}{2}\exp(-z_o/\delta)(1 + \exp(-4AD/\delta)) \quad [18]$$

Comparison with Monte Carlo

Let us compare the above analytic descriptions of R(r) and R_d with the data generated by a Monte Carlo simulation.[6] For this simulation, the optical properties of a turbid aqueous solution are chosen such that n = 1.33, μ_a = 0.5 cm^{-1}, μ_s = 100 cm^{-1}, and g = 0.9. For such a medium, the Monte Carlo simulation (100,000 photons) yields a specular reflectance of 0.020, a diffuse reflectance of 0.386, and the fraction of incident energy which is absorbed by the tissue is 0.594.

First compare the calculations of R_d. Monte Carlo yielded 0.386. Eq. 18 yields 0.427 which is 10% larger than the Monte Carlo result.

Now compare the calculations of R(r). Fig. 2 compares the results of the Monte Carlo simulation (circles) with the analytic Eq. 13 (lines). R(r) is plotted vs the dimensionless radial position, r/δ. Fig. 2A looks at the behavior relatively close to the source. There is disagreement between the Monte Carlo data and Eq. 13 near the dipole source within $r/\delta < 0.7$. Fig. 2B shows the behavior far from the source. In this case, Eq. 13 shows agreement with the Monte Carlo data distant from the dipole source.

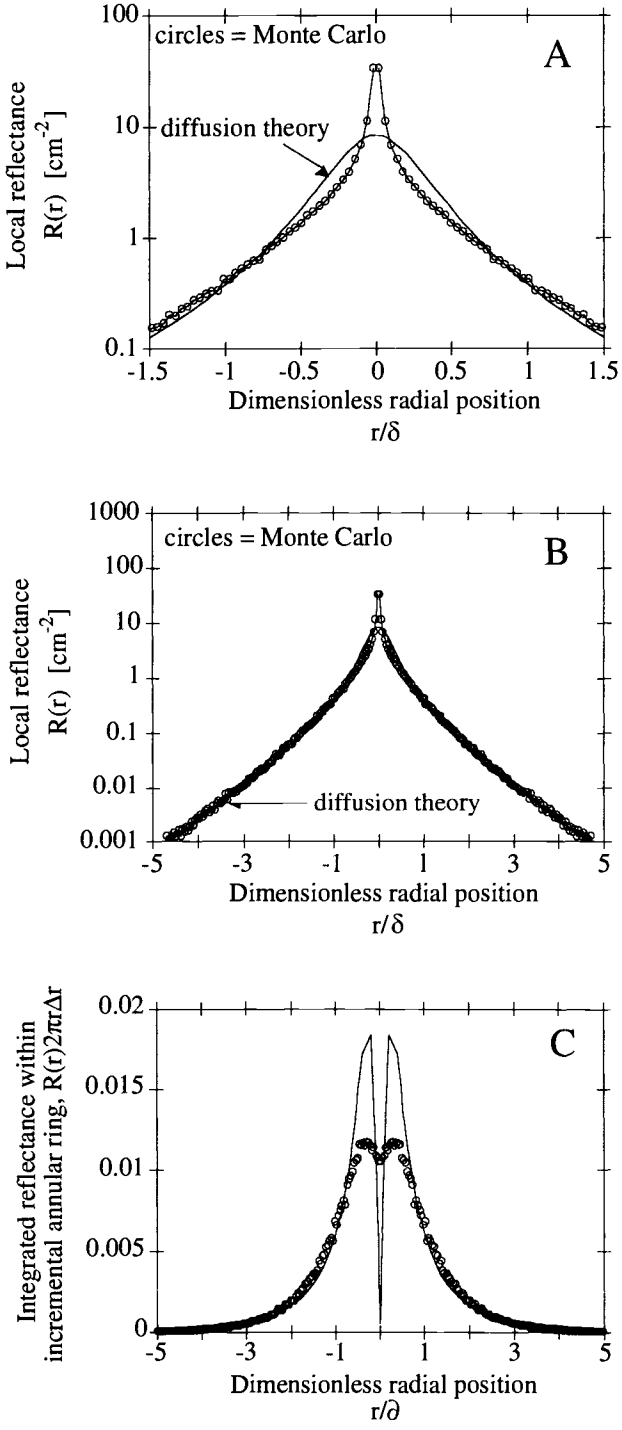

Figure 2: (legend on next page)

Figure 2: (on previous page)
Comparison of analytic curves for the local reflectance, R(r), and a Monte Carlo simulation (optical properties: $\mu_a = 0.5\ cm^{-1}$, $\mu_s = 100\ cm^{-1}$, g = 0.9, n = 1.33.) The solid lines indicate the dipole diffusion theory of Farrel et al.[3] (Eq. 13). The circles indicate a Monte Carlo simulation using 100,000 photon trajectories.

(A) R(r) is plotted vs the dimensionless radial position, r/δ. Near the point source, the diffusion theory fits for $r/\delta > 0.7$.

(B) Far from the source, Eq. 13 fits well for all the data.

(C) The total reflectance escaping within an incremental annular ring with width Δr at position r/δ is plotted. This reflectance per incremental annular ring equals $R(r)2\pi r\Delta r$, where $\Delta r = 100\ \mu m$ which was the resolution employed in the Monte Carlo simulation. Most of the energy is confined to $r/\delta \leq 4$.

Fig. 2C plots the integrated R(r) in each incremental annular ring of width $\Delta r = 100\ \mu m$ (the resolution used in the Monte Carlo simulation), which equals $R(r)2\pi r\Delta r$. Most of the energy is confined to $r/\delta < 4$. In summary, Eq. 13 offers a relatively good description of R(r) for $r/\delta > 0.7$ and most of the available signal energy occurs within $r/\delta < 4$.

In practical video reflectometry, the behavior of R(r) near a point source is not always so well behaved. It is not always true that the laser beam is sufficiently narrow to be considered a point source when the δ for tissue is small. Moreover, the behavior of R(r) distant from the source is more strongly affected by the tissue optical properties. Therefore, Eq. 13 offers an effective description of R(r) measured experimentally, especially when video camera senstivity allows the R(r) signal distant from the source to be measured reliably and the tissue thickness is sufficient to satisfy the assumption of a semi-infinite tissue. But the data near the source is not expected to exactly match Eq. 13, and should not be included in data analysis.

In the following experimental studies, we have used Eqs. 13 and 18 for the analysis. Farrell et al. have recently reported progress in the use of neural networks to analyze R(r) data.[7]

EXPERIMENTAL METHOD

The experimental measurement of a tissue or phantom tissue using video reflectometry is illustrated in Fig. 3. A narrow laser beam is directed vertically down onto the medium by a mirror. An attenuation filter can be placed at the output of the laser. A distant calibrated photodiode is positioned above the sample to collect a portion of the diffuse reflectance. A video camera is positioned to measure the pattern of local reflectance. Digitization of the video image yields R(r) data in arbitrary pixel units.

Both the probe and video camera are positioned slightly off-axis such that they will not collect the specular reflectance from the air/tissue boundary, which is a condition easily satisfied for a smooth surface but more difficult for a rough surface. Nishioka et al.[8] reported that the specular reflectance from human esophagus behaves as a Henyey-Greenstein function with an average $\cos\theta$ value or g value of ~0.7. A thin fluid or glass layer on top of the tissue can smooth the tissue surface, however such a

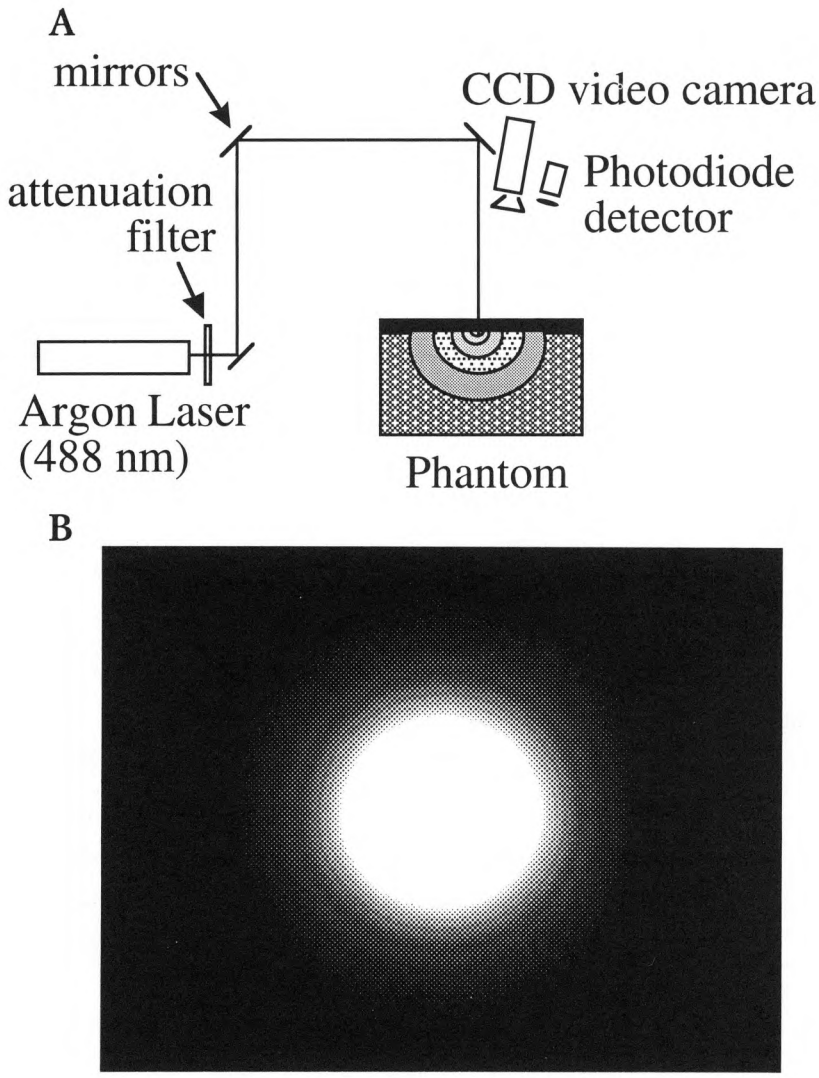

Figure 3: Video reflectometry measurement. (A) Experimental setup. A laser beam is directed down onto a tissue or phantom. Attenuation filters at the laser output control the incident laser energy. A photodiode observes a portion of the total diffuse reflectance, R_d. A video camera measures the spatial distribution of local reflectance, R(r). (B) A typical video image captured by the camera. The test object in this case is a fish tank filled with an Intralipid/trypan blue solution.

layer will artificially broaden the pattern of lateral photon migration. Specular reflectance is an issue in video reflectometry for data collected from the area where the source irradiates the tissue. If the analysis neglects this central data, specular reflectance is no longer a problem.

Total diffuse reflectance

The measurement of total diffuse reflectance is accomplished with a photodiode placed at a fixed position distant from the tissue. The distance is sufficiently large such that the angle of collection from one edge or the opposite edge of the glowball of escaping reflectance is not significantly different, therefore the collection is not influenced by any $\cos\theta$ dependence of escaping reflectance. Two measurements are made, one of a reflectance standard, M_{std}, and one of the unknown test medium, M_{test}. Their ratio specifies R_d:

$$\frac{M_{test}}{M_{std}} = \frac{SDCR_d}{SDCR_{std}} = \frac{R_d}{R_{std}} \qquad [13]$$

where S is the light source, D is the detector response, and C is the collection efficiency of the photodiode which depends on the geometry of the setup. The R_d is calculated:

$$R_d = \frac{M_{test}}{M_{std}} R_{std} \qquad [14]$$

Video camera measurement

The video camera measurement is repeated several times with different attenuation filters at the laser output. The dynamic range of the video camera will not accomodate more than 2 orders of magnitude of intensity. With no filter, the central portion of the video field will be saturated but good data at the periphery of the field will be acquired. With the strongest attenuation filter, the central portion of the field will yield good data but the periphery of the field will appear dark. We routinely acquire 5 frames using 5 attenuation filters: OD = 3, OD = 2, OD = 1, OD = 0.5, and OD = 0 (no filter), where transmission, T, equals 10^{-OD}.

The camera gain and offset controls were set such that the signal measured with the laser light blocked (no light) was at least 5 pixel units due to background lighting and the strong central signal when the OD5 filter attenuated the laser beam was only 250 pixel units. The camera must have a linear response for these experiments. If the camera has a nonlinear response, then a separate calibration curve must be generated to convert signals to a linear response. We have successfully worked with a nonlinear camera, but the calibration is bothersome. We currently use a camera with a linear response which is far more convenient, and all data in this paper involve a linear camera response.

To account for the baseline corresponding to no light, the baseline value (5 pixel units) is subtracted from the data. Then each video frame is multiplied by the inverse attenuation factor, 10^{OD}, to yield a numeric value corresponding to the R(r) signal that would be observed if the laser had not been attenuated by any filters.

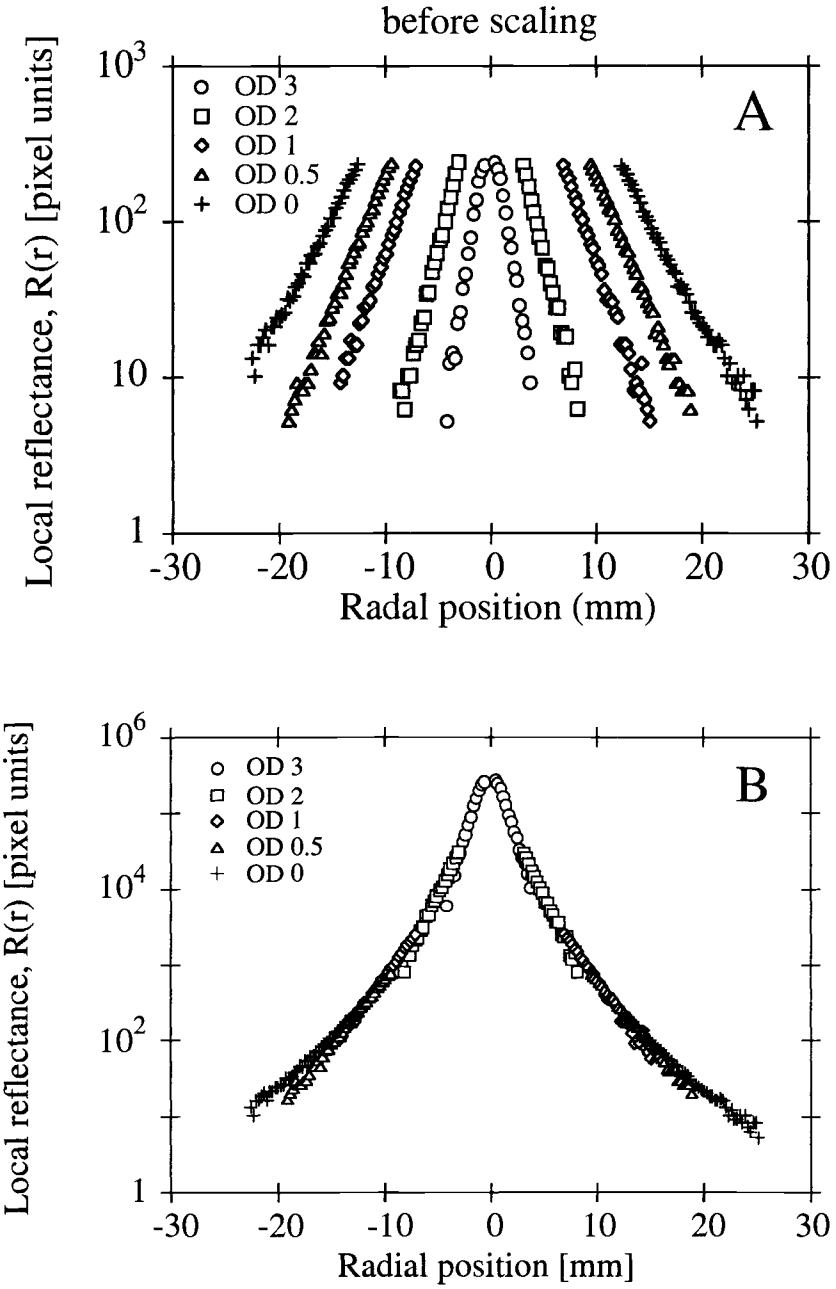

Figure 4: Video reflectometry data digitized by computer. (A) The raw data shows the R(r) data taken with a set of attenuation filters (filter transmission = 10^{-OD}). The data falls between 5 and 255 pixel units. The baseline pixel value for no light was about 5 pixel units. (B) The data after subtracting the no-light baseline and multiplying by the inverse attenuation factor, 10^{OD}. The data now span over 4 orders of magnitude.

Figure 4A illustrates the raw data taken with the 5 filters. The data acquisition utilizes the 5-255 range of pixel units, but data exceeding 250 pixel units is rejected to avoid any data by a saturated camera element. Figure 4B indicates the corrected data after subtracting the no-light baseline and scaling the raw data by the inverse attenuation factor. The data now extends over 4 orders of magnitude. If the pixel value of the no-light baseline is not carefully measured and appropriately subtracted, the lower intensity signals of each data set will strongly deviate from the data derived from stronger signals. Careful subtraction of the no-light baseline is therefore checked by observing smoothness of the final corrected curve.

Phantom experiments

To test the accuracy and reproducibility of the method, phantom tissues were created using Intralipid as the scatterer and trypan blue as the absorber. Three phantoms were prepared with different optical properties. We used the photodiode measurement of R_d and the video camera measurement of R(r) (data too close to the point source was not included in the analysis). Fig. 5 indicates a typical experimental result and the corresponding theoretical fit using Eqs. 13 and 18. The results are summarized in Table 2. The video reflectometry was able to deduce the optical properties with a relative error of less than 10%.

Table 2: Video reflectometry of tissue phantoms

	Mixture 1	Mixture 2	Mixture 3
μ_a (cm^{-1})	0.134	0.263	0.516
μ_a fit	0.139	0.271	0.494
relative error (μ_a fit - μ_a)/μ_a	3.7%	2.7%	4.3%
μ_s' (cm^{-1})	10.2	15.0	20.9
μ_s' fit	9.65	14.0	18.9
relative error (μ_s fit - μ_s)/μ_s	5.7%	6.5%	9.5%

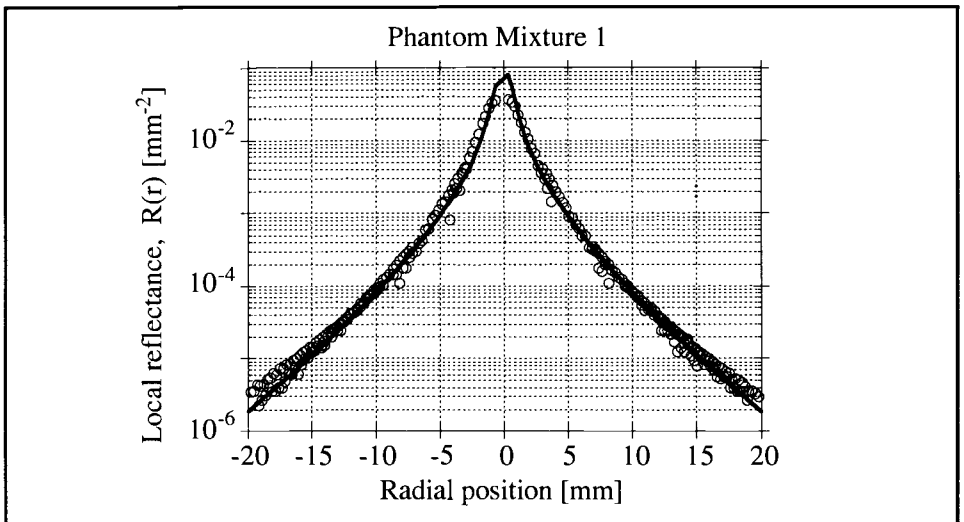

Figure 5: (Legend next page)

Figure 5: (on previous page)
Typical phantom experiment. The phantom used Intralipid as scatterer and trypan blue as absorber (μ_a = 0.134 cm^{-1}, μ_s' = 10.2 cm^{-1}, g ≈ 0.7). Separate experiments not discussed here specified the scattering and absorption properties of the stock solutions used for the constructing the phantoms. The digitized data from the video camera after correction for the attenuation filters are shown. The analytic fit using Eqs. 13 and 18 is also shown. The experimental R(r) data was normalized to ensure that Eq. 17, which relates R(r) measured by the camera and R_d measured by the photodiode, was satisfied. In this figure, R(r) is expressed as mm^{-2}.

Tissue experiments

Three experiments were attempted. One measured the combined mucosal and muscle layers of pig stomach in an *ex vivo* sample. The second measured the skin of a human forearm *in vivo*. The third measured the exposed leg muscle of an anesthetized rat *in vivo*. The measurements and analytical fit are shown in Figs. 6, 7, and 8. The optical properties from these three experiments are summarized in Table 3. Note that the absorption coefficients cited in Table 3 are rather low compared to previously cited optical properties. We believe that video reflectometry is yielding more accurate measurements of μ_a than other methods such as integrating spheres where unaccounted losses can yield overestimates for μ_a.

Figure 8 shows the result for the rat muscle. The data shows a marked deviation at a radial distance of about 2 mm from the source. The thickness of this muscle was only a few mm. Such behavior is probably due to the underlying tissue having different optical properties than the muscle itself. Analysis of such results can yield the thickness of the muscle layer and the optical properties of the underlying layer, although we do not attempt such an exercise in this paper.

Table 3: Optical properties measured by video reflectometry.

	λ (nm)	μ_a(cm^{-1})	μ_s' (cm^{-1})	δ (cm)
pig stomach (ex vivo)	805	0.16	20	0.321
human skin (in vivo)	805	0.085	29	0.367
rat muscle (in vivo)	633	0.36	11	0.285

SUMMARY

Video reflectometry offers a noncontact method of measuring optical properties. The accuracy appears to be within 10% error. The ability to nondestructively measure *in vivo* tissue sites allows measurements of tissues with their natural water balance and blood content.

ACKNOWLEDGEMENTS

This work was supported by the National Institutes of Health (R29-HL45045) and the Medical Free Electron Laser Program of the Office of Naval Research (N00015-91J-1354).

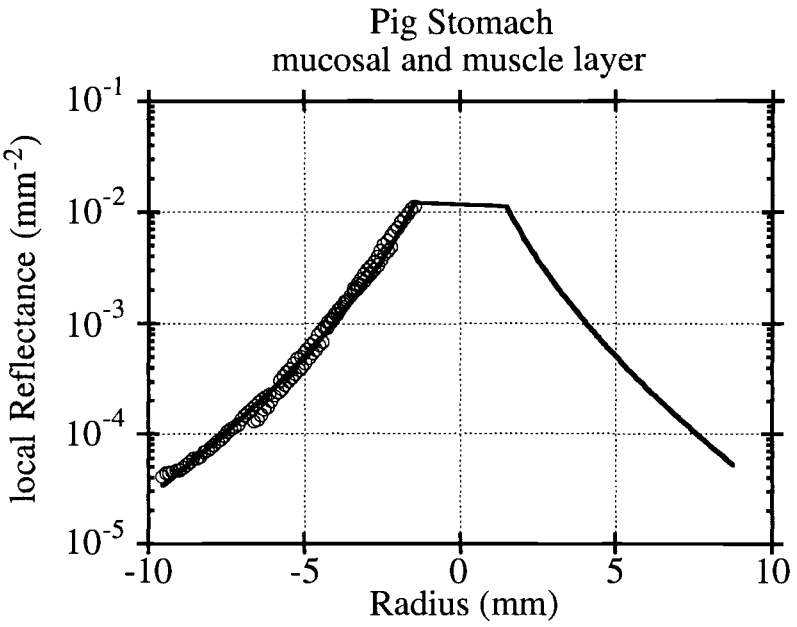

Figure 6: Video reflectometry of *ex vivo* pig stomach, combined mucosa and muscle layers (805 nm wavelength from a diode laser, $\mu_a = 0.16$ cm^{-1}, $\mu_s' = 20$ cm^{-1}).

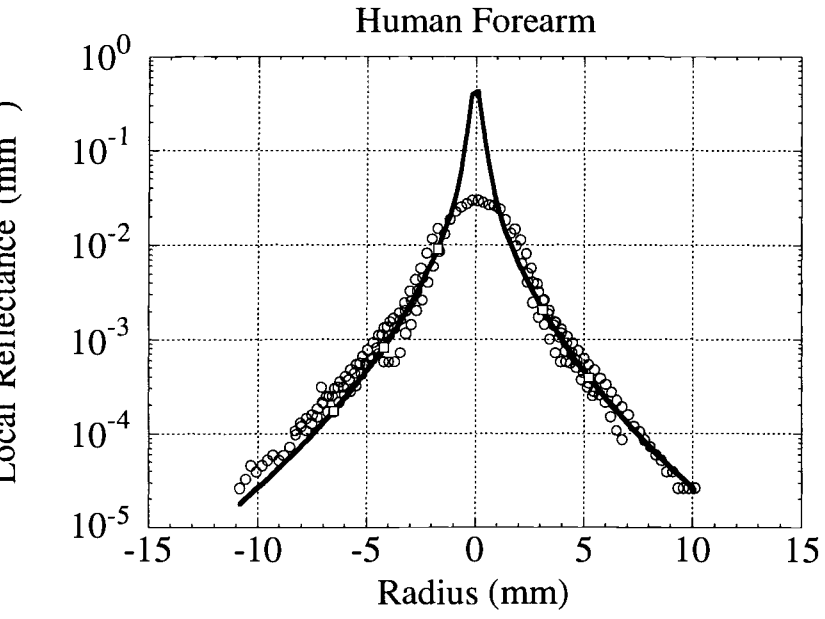

Figure 7: Video reflectometry of *in vivo* human forearm (805 nm wavelength from a diode laser, $\mu_a = 0.085$ cm^{-1}, $\mu_s' = 29$ cm^{-1}).

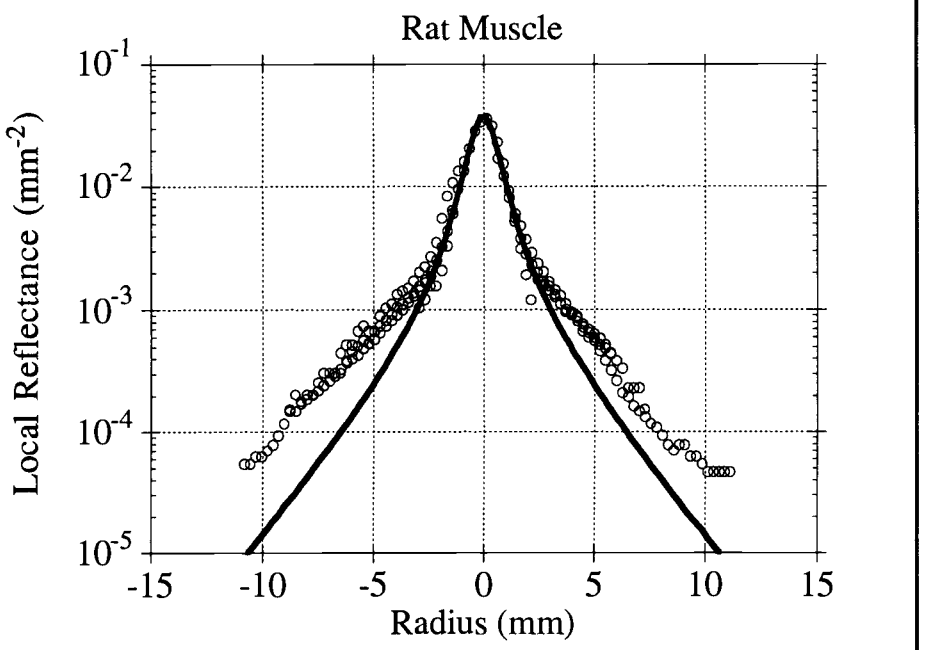

Figure 8: Video reflectometry of *in vivo* rat leg muscle (633 nm wavelength from HeNe laser, μ_a = 0.36 cm^{-1}, μ_s' = 11 cm^{-1}). The deviation at r > 2 mm is probably due to the influence of the underlying tissue layer because the leg muscle was only a few mm thick.

REFERENCES

1. T. J. Farrel, M. S. Patterson, B. Wilson, "A diffusion theory model of spatially resolved, steady-state diffuse reflectance for the noninvasive determination of tissue optical properties *in vivo*," *Med. Phys.* 19:881-888 (1992).

2. R. A. J. Groenhuis, H. A. Ferwerda, J. J. T. Bosch, "Scattering and absorption of turbid materials determined from reflection measurements. 1: Theory," *App. Opt.* 22:2456-2462 (1983).

3. S. L. Jacques, "Simple theory and rules of thumb for dosimetry during photodynamic therapy. in *SPIE Proceedings, Photodynamic Therapy: Mechanisms*, Vol 1065, ed. T. Dougherty (1989).

4. D. R. Wyman, M. S. Patterson, B. C. Wilson, "Similarity relations for the interaction parameters in radiation transport," *App. Opt.* 28:5243-5349 (1989).

5. L. Wang, S. L. Jacques, "Analysis of diffusion theory and similarity relations for light reflectance by turbid media," in *SPIE Proceedings, Photon Migration and Imaging in Random Media and Tissues*, Vol. 1888 (1993).

6. L. Wang, S. L. Jacques: *Monte Carlo Modeling of Light Transport in Multi-layered Tissues in Standard C.* Software and 131-page manual. Published by Laser Biology Research Laboratory, Univ. of Texas M. D. Anderson Cancer Center, 1515 Holcombe Blvd., Houston, TX 77030, USA, email: slj@laser.mda.uth.tmc.edu (1992).

7. T. J. Farrel, B. C. Wilson, M. S. Patterson, "The use of a neural network to determine tissue optical properties from spatially resolved diffuse reflectance measurements," *Phys. Med. Biol.* 37:2281-2286 (1992).

8. N. S. Nishioka, S. L. Jacques, J. M. Richter, R. R. Anderson, "Reflection and transmission of light from the esophagus: The influence of incident angle," *Gasteroenterology* 94:1180-1185 (1988).